A Quantitative Study of the Composition of $Sm(Co_{0.68}Fe_{0.20}Cu_{0.10}Zr_{0.02})_{7.5}$ Alloy by 3D Atom-Probe Analysis

X.Y. Xiong[a] and T.R. Finlayson[b]

[a] *Department of Materials Engineering, Monash University, Victoria 3800, Australia.*
[b] *School of Physics, Monash University, Victoria 3800, Australia.*

3D atom-probe analysis of the composition of a SmCoFeCuZr alloy was conducted in a temperature range from 65 to 10.6K. The optimum probing temperature giving the best measurement of the composition, was found to be about 20K. At a higher probing temperature significant preferential evaporation of Sm atoms occurred due to the very low evaporation field of Sm, which was found to be 15.2V/nm using the charge exchange model.

1. Introduction

Three-dimensional, atom-probe, field-ion microscopy (APFIM), is a unique technique to analyse the compositions of nanometer-scale precipitates and clusters in alloys and composites [1,2]. However, to do quantitative, compositional analysis using the 3D atom-probe (3DAP) for a new alloy system, appropriate experimental conditions must selected to avoid possible preferential evaporation or retention of one species from the specimen surface, as different elements have different field-evaporation potentials in the alloy. The measured composition varies with the following important experimental parameters: (a) the temperature of the specimen; (b) the pulse fraction; (c) the orientation of the specimen; and (d) the field-evaporation rate. Previous studies on various alloys [1] have demonstrated that for the pulse fraction it is safe to use >15% to achieve an equal detection efficiency for each element in the alloy. For the orientation of the specimen, the probing direction could be close to but not on the low-index poles, to obtain correct compositions. For the field-evaporation rate, it is suggested that a low rate (< 0.02 ions per pulse) should be used to avoid possible ion pile-up at the detector. As for the temperature, a range from 20 to 70K was used for various materials.

The SmCo-based permanent magnets have superior high temperature magnetic properties. The changes in the local compositional distribution on a nanometer scale in the complicated microstructure during heat treatment are not yet fully understood. Careful 3DAP analysis is needed. The purpose of this work is to determine a right temperature for analysing a $Sm(Co_{0.68}Fe_{0.20}Cu_{0.10}Zr_{0.02})_{7.5}$ alloy in a single phase state with the $SmCo_7$ structure, so that the compositions of more complicated microstructures of this alloy after heat treatment, can be estimated correctly in our further investigations of the effects of heat treatment on alloy constitution and phase compositions. The effect of probing temperature on the measured composition is discussed, based on the evaporation fields.

2. Experimental

An alloy ingot of the composition $Sm(Co_{0.68}Fe_{0.20}Cu_{0.10}Zr_{0.02})_{7.5}$ was prepared using an Ar arc furnace. Ribbon samples were made using a single-roller, melt-spinning technique under a controlled inert-gas atmosphere. Chemical analysis of the ribbon samples confirmed that the real composition of the alloy was similar to the nominal composition, shown in Table 1. The microstructure was examined using XRD and TEM (Philips CM20). 3DAP specimens were prepared by grinding ribbons into square rods of 20μm×20μm×8mm and electropolishing the square rod to a sharp tip. 3DAP analysis was conducted in ultrahigh vacuum ($<10^{-8}$Pa) using an Oxford NanoScience 3DAP field-ion microscope [3]. The pulse fraction was 20% and the pulse repetition rate was 1500Hz. The evaporation rate was in the range of 0.002 to 0.01 ions per pulse.

Table 1. Compositions of the $Sm(Co_{0.68}Fe_{0.20}Cu_{0.10}Zr_{0.02})_{7.5}$ alloy ribbons.

Composition	Sm	Co	Fe	Cu	Zr
Nominal, at.%	11.76	60.00	17.65	8.82	1.77
Measured, at.%	10.78	60.32	17.25	9.87	1.79

3. Results and Discussions

The XRD analysis of the as-spun ribbons showed that the alloy comprised a single phase with the $SmCo_7$ structure. A TEM micrograph from an as-spun ribbon is given in Fig. 1, showing fairly large grain structure. The atom probe test showed uniform distribution of atoms for each element. The

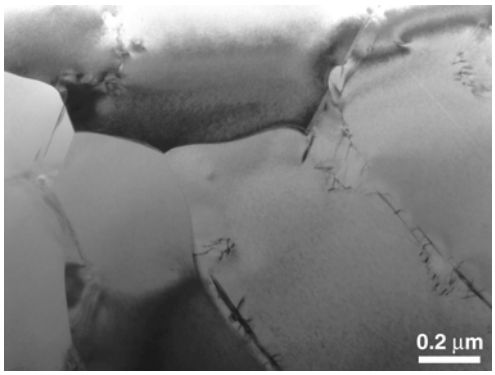

Fig. 1. TEM micrograph of an as-spun $Sm(Co_{0.68}Fe_{0.20}Cu_{0.10}Zr_{0.02})_{7.5}$ alloy ribbon.

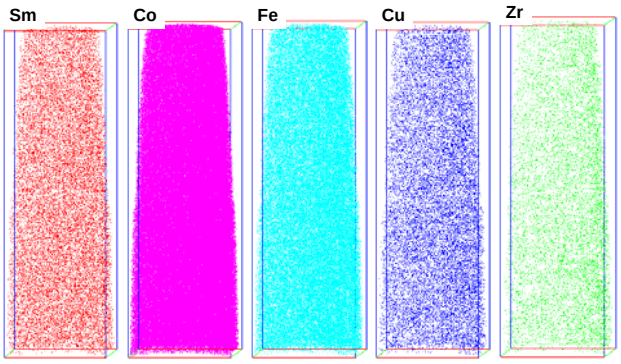

Fig. 2. 3D atom maps of the tip probed at 65K. The box size is 16×16×53 nm^3.

raw data size of each test was around 900,000 ions. A typical set of atom maps for the tip probed at 65K is shown in Fig. 2.

The measured concentrations as functions of probing temperature are given in Fig. 3. It can be seen that the measured concentrations of Fe, Cu and Zr atoms do not change much over the whole temperature range, but the concentrations of Sm and Co atoms vary significantly as the probing temperature decreases from 65 to 10.6K. The Sm concentration increased from 5.44±0.04at.% at 65K to 12.12±0.04at.% at 10.6K, while the Co concentration decreased from 67.18±0.07at.% at 65K to 59.81±0.06at.% at 10.6K. In comparison with the chemical analysis results in Table 1, it is found that the measured concentrations of Sm and Co at 65K were far from the true values. Only when the temperature is between 15 and 20K are the measured concentrations of Sm and Co equal to the true values, while the measured concentrations of Fe, Cu and Zr are 19.46±0.07at.%, 6.24±0.04at.% and 2.16±0.02at.%, respectively. The Cu concentration is consistently lower than the true value by about 3at.%, while the Fe concentration is higher than the true value by about 2at.%. The Zr concentration is not much different from the true value. It seems that when the probing temperature was 65K, the preferential evaporation of Sm occurred during the probing. This preferential evaporation of Sm was alleviated when the specimen temperature was decreased to about 20K. The Cu atoms were also preferentially evaporated to some lower extent which was not changed with decreasing temperature, while the Fe atoms were preferentially retained slightly during the probing and the preferential retention remained unchanged at lower temperatures.

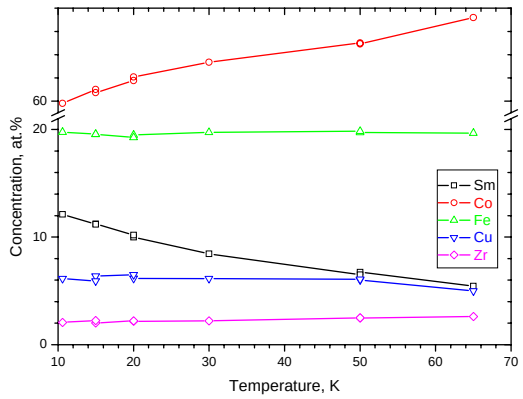

Fig. 3. Measured concentrations as a function of probing temperature.

To understand the above field evaporation behavior, the evaporation fields of the pure metals have been used, as the data for the elements in alloys are not available. It is assumed that the evaporation field of the atom in the alloy is not much different from that in the corresponding metal. Table 2 lists the evaporation fields, F_n, in bold, for Fe, Co, Cu, Zr and Sm pure metals. The data for Fe, Co, Cu and Zr are from Müller and Tsong's books [4,5]. The evaporation field data for Sm are not available from the literature and are calculated by following the charge exchange model for which the evaporation field, F_n, is [5]:

$$F_n = \frac{1}{nr_0}(\Lambda + \sum I_n - n\Phi - \frac{3.6n^2}{r_0}) \text{ V/Å},$$

where Λ is the sublimation energy in eV, I_n the nth ionization potential in eV, Φ the work function in eV and r_0 the single bond atomic radius of the metal atoms. For convenience of comparison, the energy parameters of these metals and their melting points are listed in Table 2. The Sm evaporation field estimated from the image hump model [5] is also given in Table 2, showing that the values obtained from the two models are similar.

Table 2. Charge exchange model predictions of low temperature evaporation fields and observed evaporation fields, F_{ob}, and melting points, T_m, for the metals.

Metal	Λ, eV	I_1, eV	I_2, eV	I_3, eV	I_4, eV	Φ, eV	r_0, Å	F_1, V/nm	F_2, V/nm	F_3, V/nm	F_4, V/nm	F_{ob}, V/nm	T_m, K
Fe	4.13	7.87	16.18	30.651	54.8	4.17	1.17	40.6	**32.2**	53.1	102.0	35	1811K
Co	4.4	7.86	17.05	33.5	51.3	4.4	1.162	41.0	**34.9**	62.3	101.0	36	1768K
Cu	3.5	7.724	20.286	36.83	55.2	4.55	1.176	**30.7**	43.2	76.9	119.8	30	1358K
Zr	6.33	6.84	13.13	22.99	34.34	4.12	1.454	45.2	**28.0**	33.6	47.3	25	2128K
*Sm	2.142	5.6436	11.07	23.4	41.4	2.7	1.8041	17.1	**15.2**	29.9	56.7		1345K
**Sm								18.0	**15.8**	30.1	57.7		

* The related data for Sm are from reference 6. ** Estimated from the image hump model.

It can be seen from Table 2 that the most abundant ion species for Fe, Co, Zr and Sm are doubly charged, and singly charged for Cu, which is consistent with the observed mass spectra in the experiment. In addition, the observed evaporation fields, F_{ob}, support the predicted evaporation field values. The calculated evaporation field of Sm, 15.2V/nm, is nearly half of those of other elements in the alloy. This explains why Sm was observed to evaporate preferentially at 65K. It is likely that the very low evaporation field of Sm allowed Sm atoms to evaporate between pulses, making some Sm atoms undetected and uncounted for the calculation. Since Sm has a stronger dependence of evaporation field on temperature, as predicted by the charge exchange model (the melting point of Sm is much lower than those of the other metals), a larger increase in the evaporation field at lower temperature is expected, and the difference in the evaporation fields of these elements becomes small, so that the preferential evaporation is prevented from occurring. It seems that the temperature dependences of evaporation fields for Fe, Cu and Zr are similar to each other, as the measured concentrations are nearly unchanged over the whole temperature range.

4. Summary

The effect of probing temperature on the compositional analysis results for a $Sm(Co_{0.68}Fe_{0.20}Cu_{0.10}Zr_{0.02})_{7.5}$ alloy using 3DAP has been examined in the range from 65 to 10.6K. The results showed that when the probing temperature was around 20K, the quantitative analysis of the composition gave reasonably good estimates. When the temperature was higher, serious preferential evaporation of Sm atoms occurred due to the very low evaporation field of Sm, which was estimated to be 15.2V/nm using the charge exchange model.

Acknowledgment

Funding for this project from the Australian Research Council is acknowledged.

References

[1] M.K. Miller, *Atom probe tomography: analysis at the atomic level* (Kluwer Academic, 2000) p85.
[2] K. Hono, *Acta mater.*, **47**, 3127 (1999).
[3] A. Cerezo, T.J. Godfrey, S.J. Sibrandij, P.J. Warren, G.D.W. Smith, *Rev Sci Instrum.*, **69**, 49 (1998).
[4] E.W. Müller and T.T. Tsong, *Field Ion Microscopy, Principles and Applications*, (Elsevier, Amsterdam, 1965) p72.
[5] T.T. Tsong, *Atom Probe Field Ion Microscopy* (Cambridge University Press, 1990) p38.
[6] David R. Lide, ed., *CRC Handbook of Chemistry and Physics, Internet Version 2005*, <http://www.hbcpnetbase.com>, CRC Press, Boca Raton, FL, pages4-112, 4-115, 10-179 and 12-124.